Supplementary Information

Impact of substituent position on crystal structure and photoconductivity in 1D and 2D lead(II) benzenethiolate coordination polymers

Ryohei Akiyoshi,*[a] Akinori Saeki,[b] Kazuyoshi Ogasawara,[a] Daisuke Tanaka*[a]

[a] Department of Chemistry, School of Science, Kwansei Gakuin University, 1 Gakuen, Sanda, Hyogo 669-1337, Japan

[b] Department of Applied Chemistry, Graduate School of Engineering, Osaka University, 2-1 Yamadaoka, Suita, Osaka 565-0871, Japan

Table of Contents

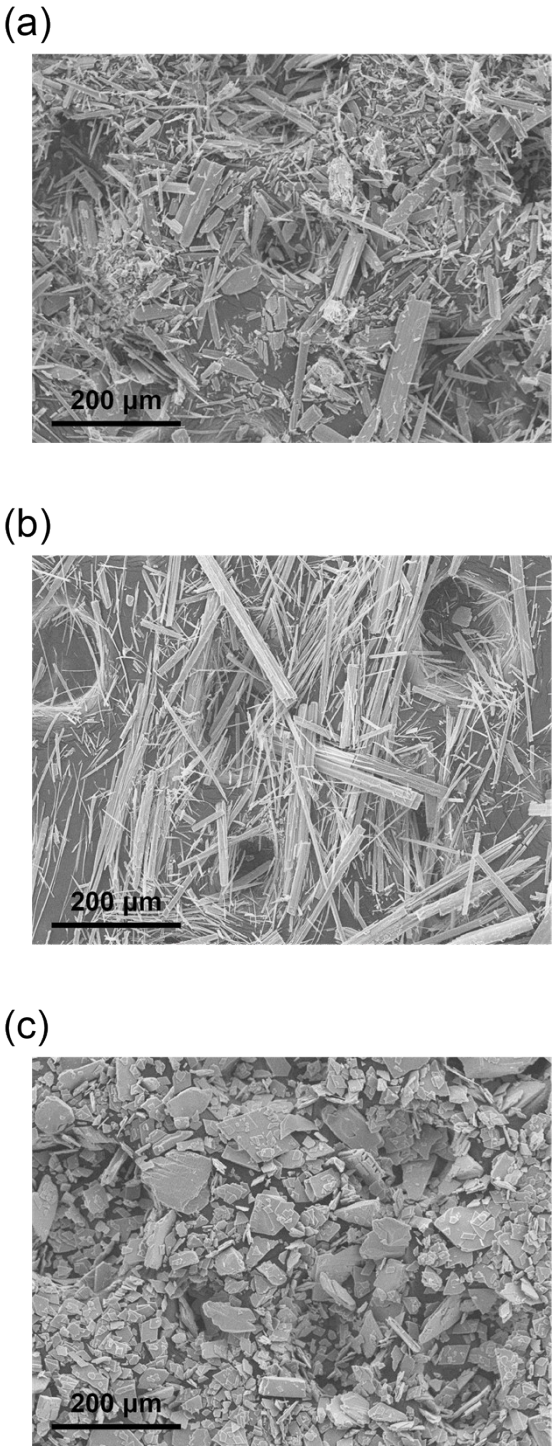

Fig. S1. SEM textures of (a) **KGF-32**, (b) **KGF-33**, and (c) **KGF-34**.

Table S1. Crystallographic data for **KGF-32**, **KGF-33**, and **KGF-34**.

Compound	**KGF-32**	**KGF-33**	**KGF-34**
Formula	$C_{14}H_{14}O_2PbS_2$	$C_{14}H_{14}O_2PbS_2$	$C_{14}H_{14}O_2PbS_2$
Formula weight	485.56	485.56	485.56
T / K	150	150	150
Crystal system	Monoclinic	Monoclinic	Monoclinic
Space group	$P2_1/c$	$P2_1/c$	$P2/n$
a / Å	9.5333 (3)	4.1327 (2)	7.6715 (4)
b / Å	19.6388 (5)	31.0738 (11)	5.1900 (2)
c / Å	7.7462 (3)	11.0299 (4)	34.4254 (13)
α / deg	90	90	90
β / deg	95.886 (3)	95.467 (4)	90.992 (4)
γ / deg	90	90	90
V / Å^3	1456.28	1410.00 (10)	1370.44 (10)
Z	4	4	4
ρ_{calc} / g cm^{-3}	2.236	2.287	12.609
μ / mm^{-1}	11.987	12.255	12.609
F_{000}	912.0	912.0	912.0
R_1 ($I > 2\sigma(I)$)	0.0194	0.0370	0.0344
R_1 (all data)	0.0234	0.0430	0.0425
wR_2 ($I > 2\sigma(I)$)	0.0456	0.0874	0.0855
wR_2 (all data)	0.0474	0.0907	0.0906
GOF	1.030	1.079	1.122
CCDC number	2308865	2308866	2308867

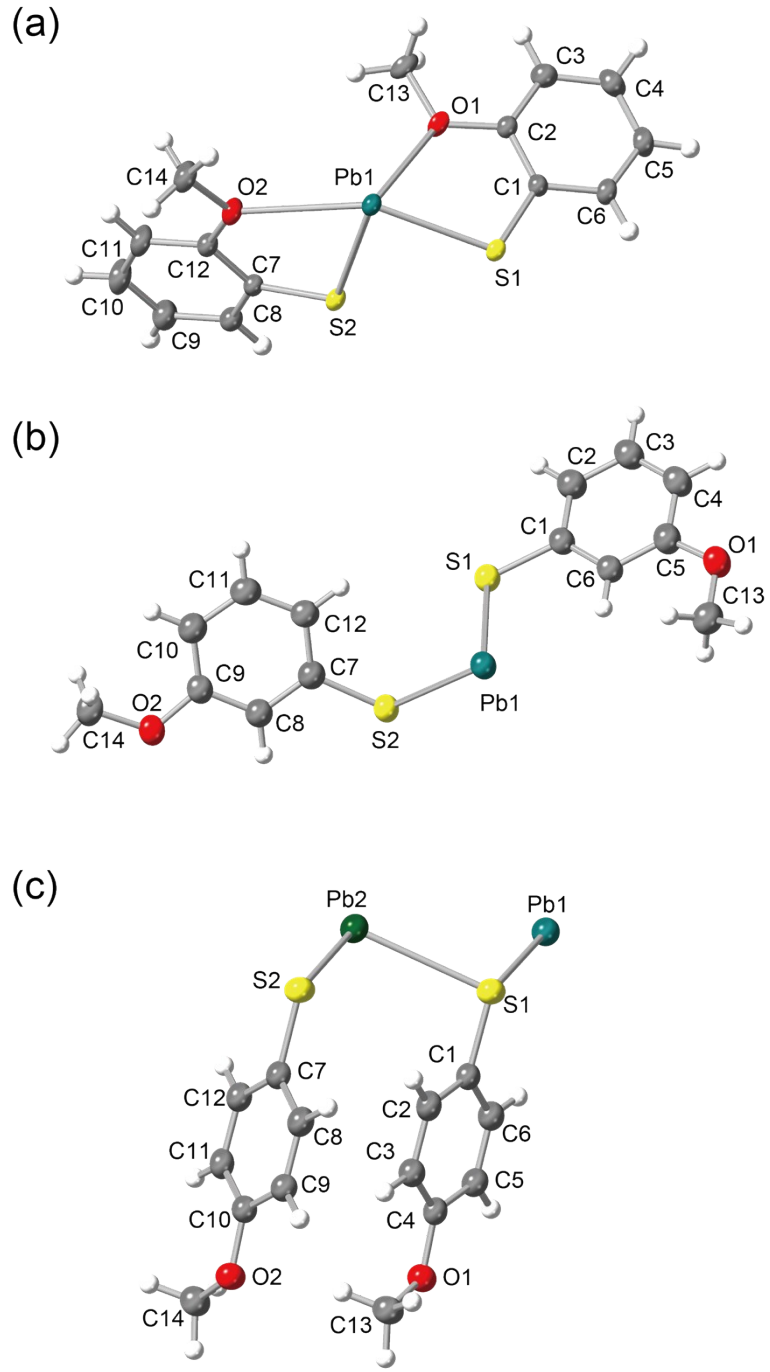

Fig. S2. Asymmetric units of (a) **KGF-32**, (b) **KGF-33**, and (c) **KGF-34**.

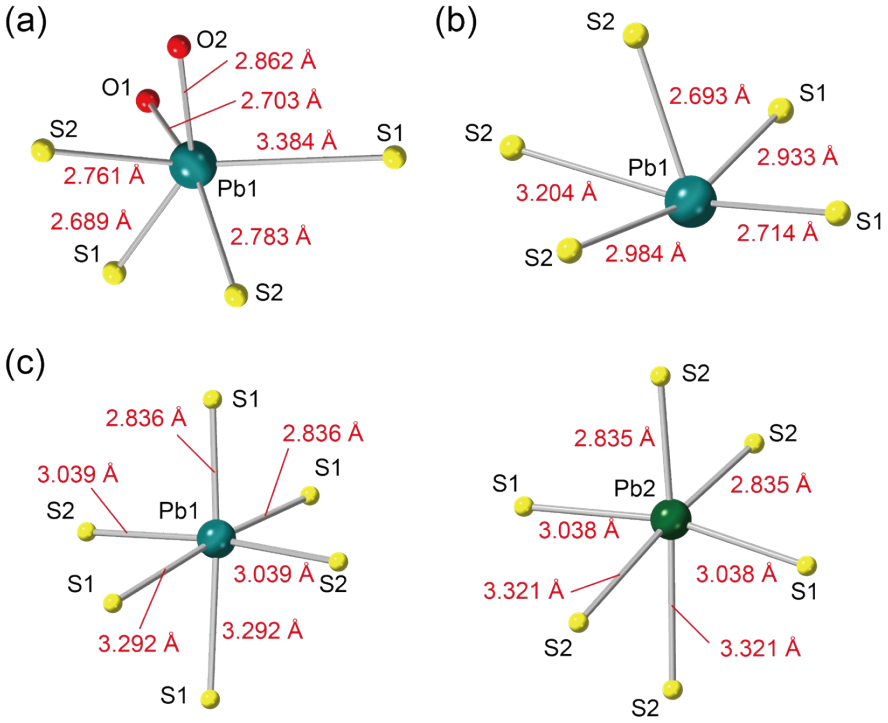

Fig. S3. Pb–S and Pb–O bond lengths of (a) **KGF-32**, (b) **KGF-33**, and (c) **KGF-34**.

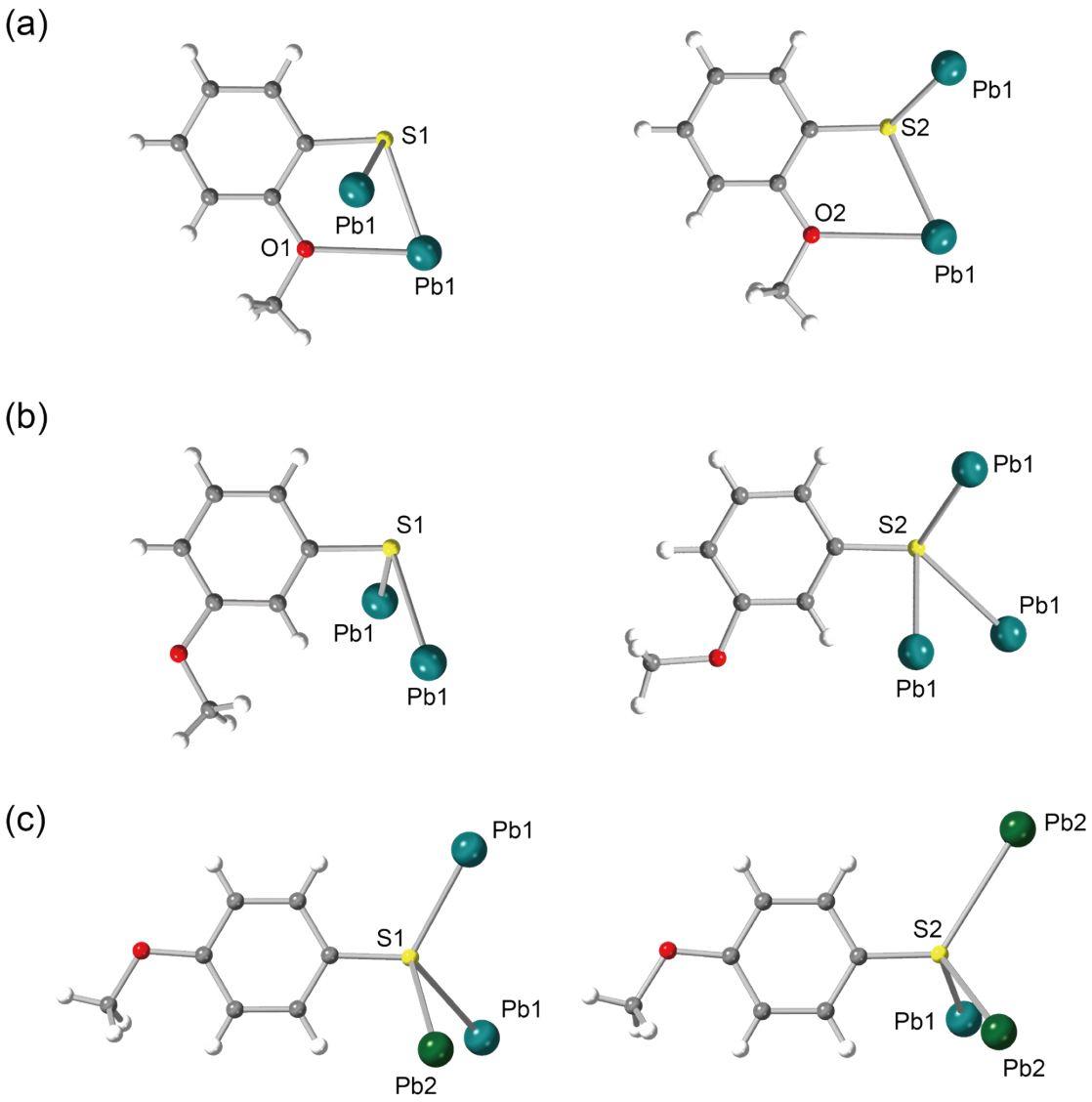

Fig. S4. Coordination mode of $SPhOMe^{-}$ anions of (a) **KGF-32**, (b) **KGF-33**, and (c) **KGF-34**.

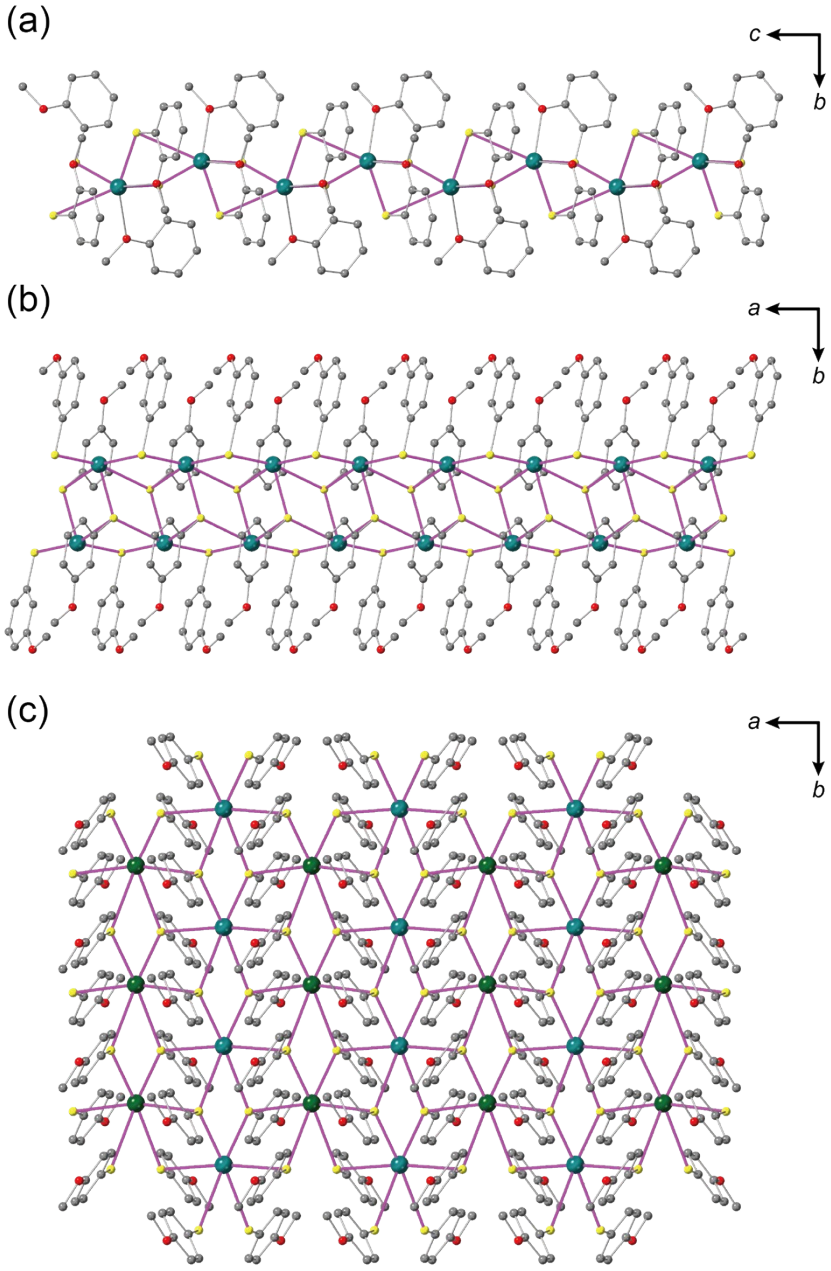

Fig. S5. Crystal structures focusing on the (–Pb–S–)$_n$ network in (a) **KGF-32**, (b) **KGF-33**, and (c) **KGF-34**. Pb–S bond is colored purple.

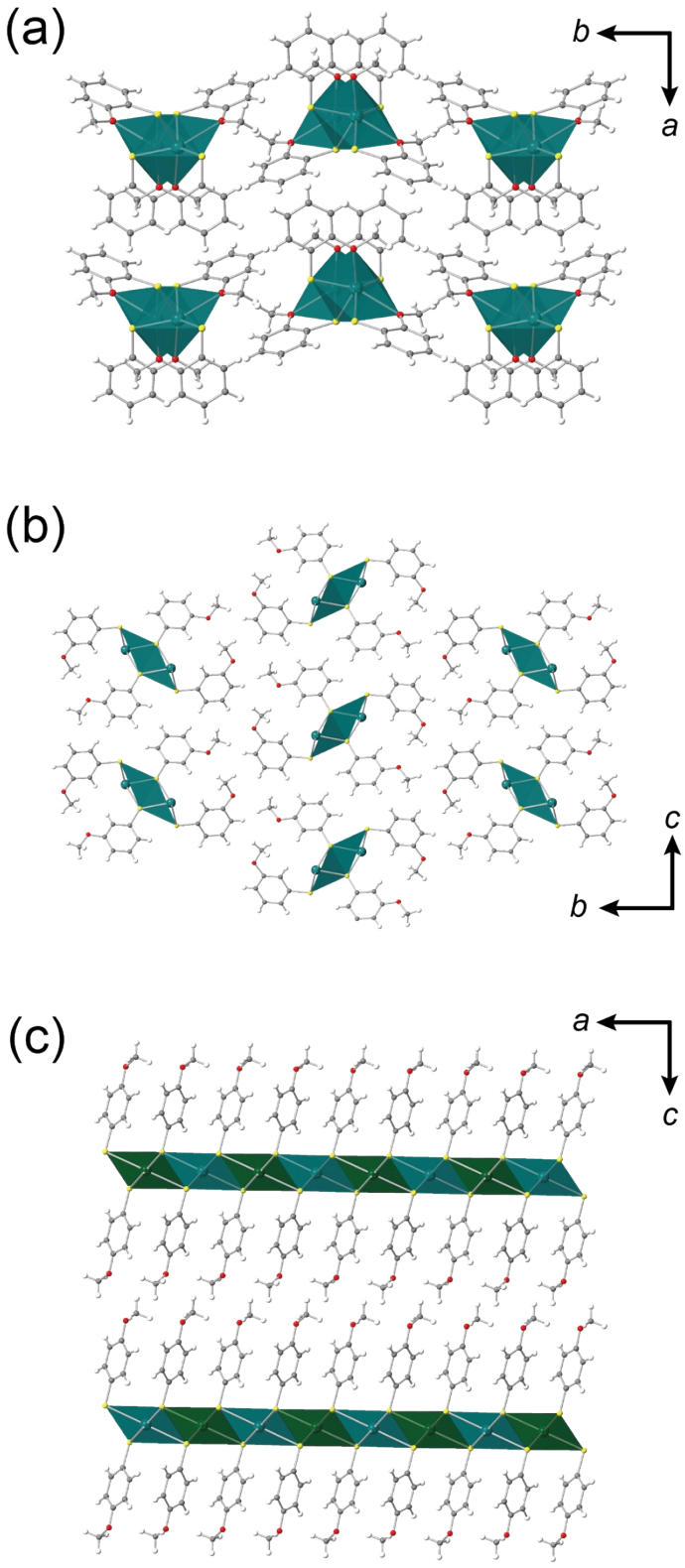

Fig. S6. Packing structures of (a) **KGF-32**, (b) **KGF-33**, and (c) **KGF-34**.

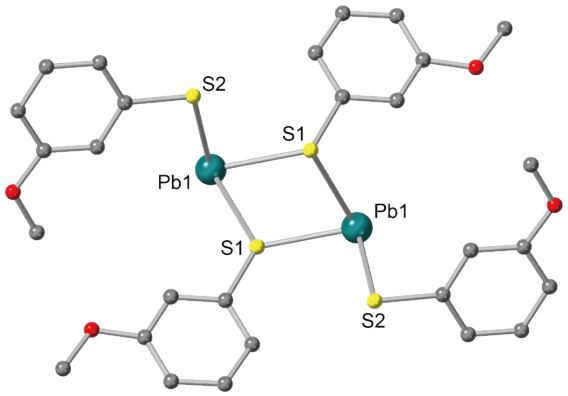

Fig. S7. Dinuclear coordination unit of **KGF-33**.

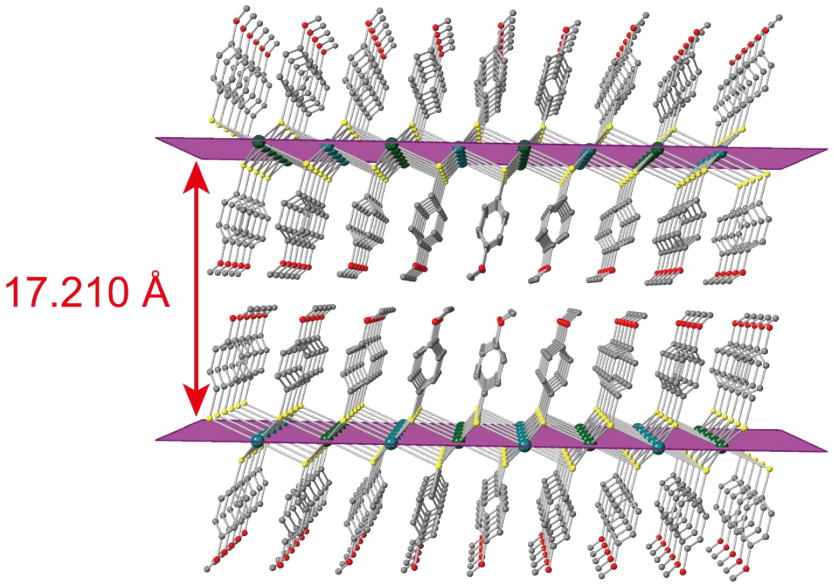

Fig. S8. Interlayer distance between 2D layers for **KGF-34**.

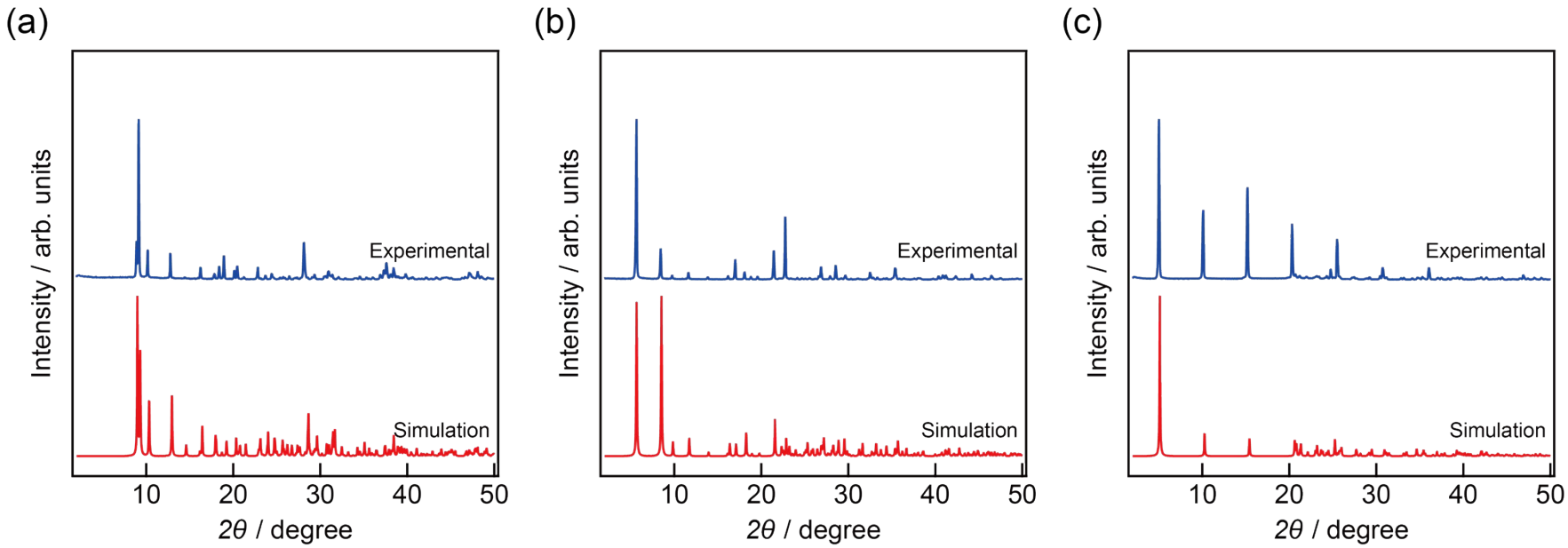

Fig. S9. PXRD patterns of (a) **KGF-32**, (b) **KGF-33**, and (c) **KGF-34** (red: Experimental, blue: Simulation).

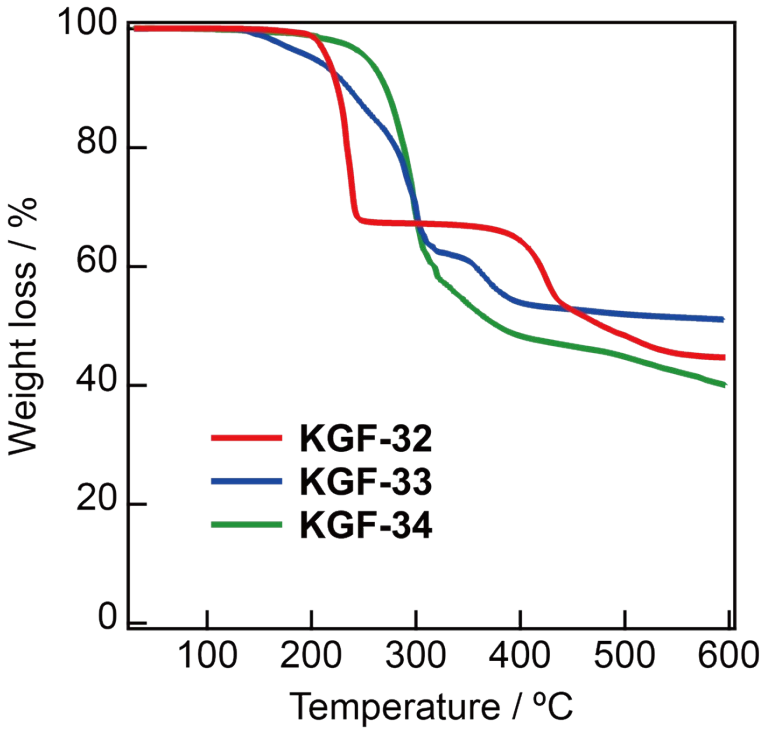

Fig. S10. TGA results for **KGF-32** (red), **KGF-33** (blue), and **KGF-34** (green) in the temperature range 30–600 °C at 10 °C min^{-1}.

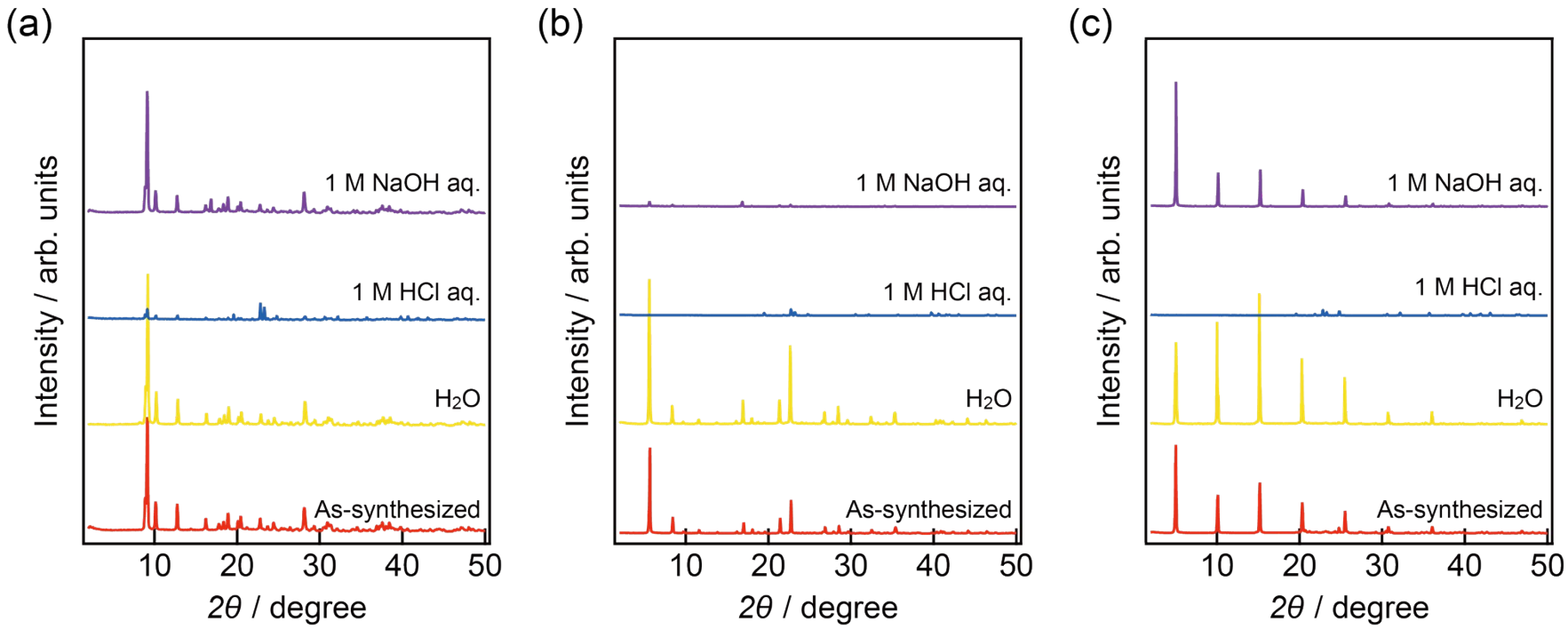

Fig. S11. Chemical stability of (a) **KGF-32**, (b) **KGF-33**, and (c) **KGF-34** toward water, 1 M HCl aq, and 1 M NaOH aq.

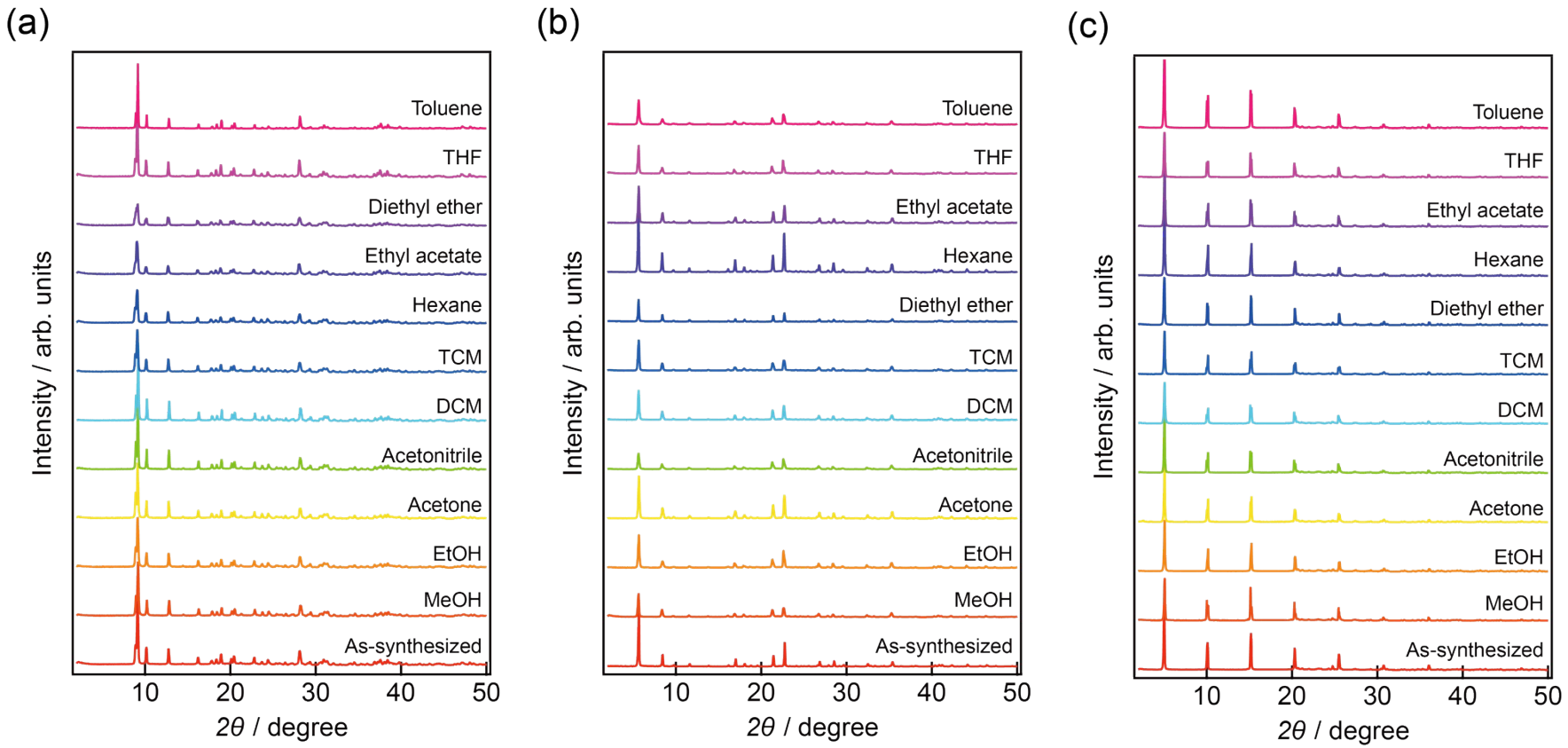

Fig. S12. Chemical stability of (a) **KGF-32**, (b) **KGF-33**, and (c) **KGF-34** toward various organic solvents. PXRD patterns were collected after soaking in methanol (MeOH), ethanol (EtOH), acetone, acetonitrile, dichloromethane (DCM), trichloromethane (TCM), hexane, ethyl acetate, diethyl ether, tetrahydrofuran (THF), and toluene.

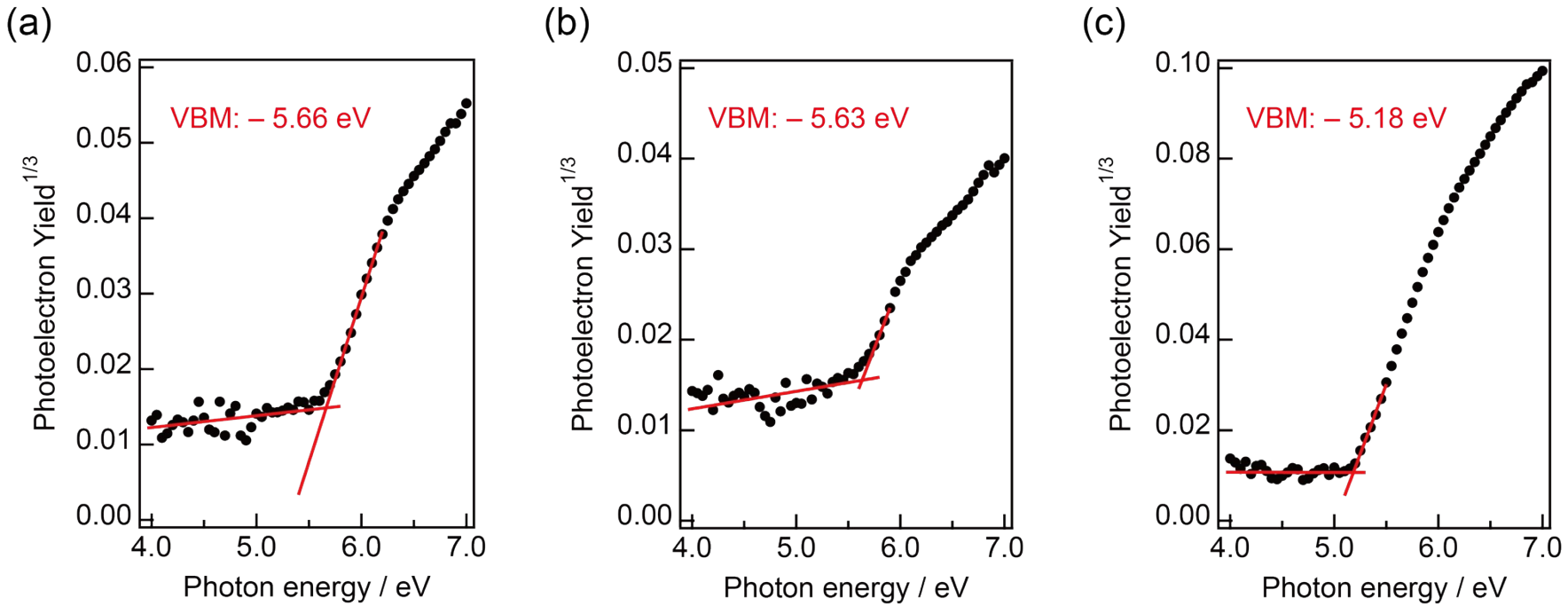

Fig. S13. PYS results for (a) **KGF-32**, (b) **KGF-33**, and (c) **KGF-34**.

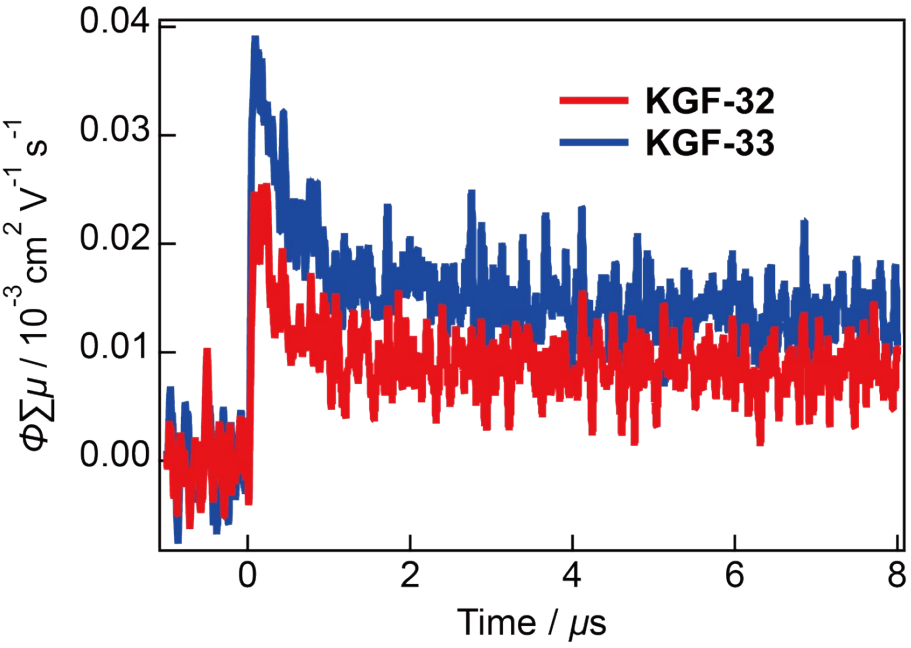

Fig. S14. TRMC results for **KGF-32** (red) and **KGF-33** (blue).

Table S2. TRMC results obtained for photoconductive S-CPs (λ_{ex} = 355 nm, I_0 = 9.1 × 10^{15} photons cm^{-2}).

Compound	$\varphi\Sigma\mu_{max}$ / cm^2 V^{-1} s^{-1}	Reference
$[Pb_3ttc_2 \cdot 2H_2O]_n$	7.4 ×10^{-5}	S1
$[Pb(tadt)]_n$	4.9 × 10^{-5}	S2
$[Sn_2(Httc)_2 \cdot MeOH]_n$	1.8 × 10^{-5}	S3
$[Ag_2Httc]_n$	2.7 × 10^{-5}	S4
$[AgH_2ttc]_n$	2.8 × 10^{-5}	S4
$[Ag_3ttc]_n$	1.5 × 10^{-4}	S4
$[Ag(tzdt)]_n$	3.6 × 10^{-5}	S5
$[Ag_2(tzdt)(TFA)]_n$	2.2 × 10^{-5}	S5
$Mn_2(DSBDC)$	1.8 × 10^{-5}	S6
$Cu_4^{I}Cu_2^{II}Br_4(pyr\text{-}dtc)_4$	3.0 × 10^{-5}	S6
$[Pb(o\text{-}SPhOMe)_2]_n$ (**KGF-32**)	2.5 × 10^{-5}	This work
$[Pb(m\text{-}SPhOMe)_2]_n$ (**KGF-33**)	3.8 × 10^{-5}	This work
$[Pb(p\text{-}SPhOMe)_2]_n$ (**KGF-34**)	1.4 × 10^{-3}	This work

H_3ttc = trithiocyanuric acid, H_2tadt = 1,3,4-thiadiazole-2,5- dithiol, Htzdt = 1,3-thiazolidine-2-thione

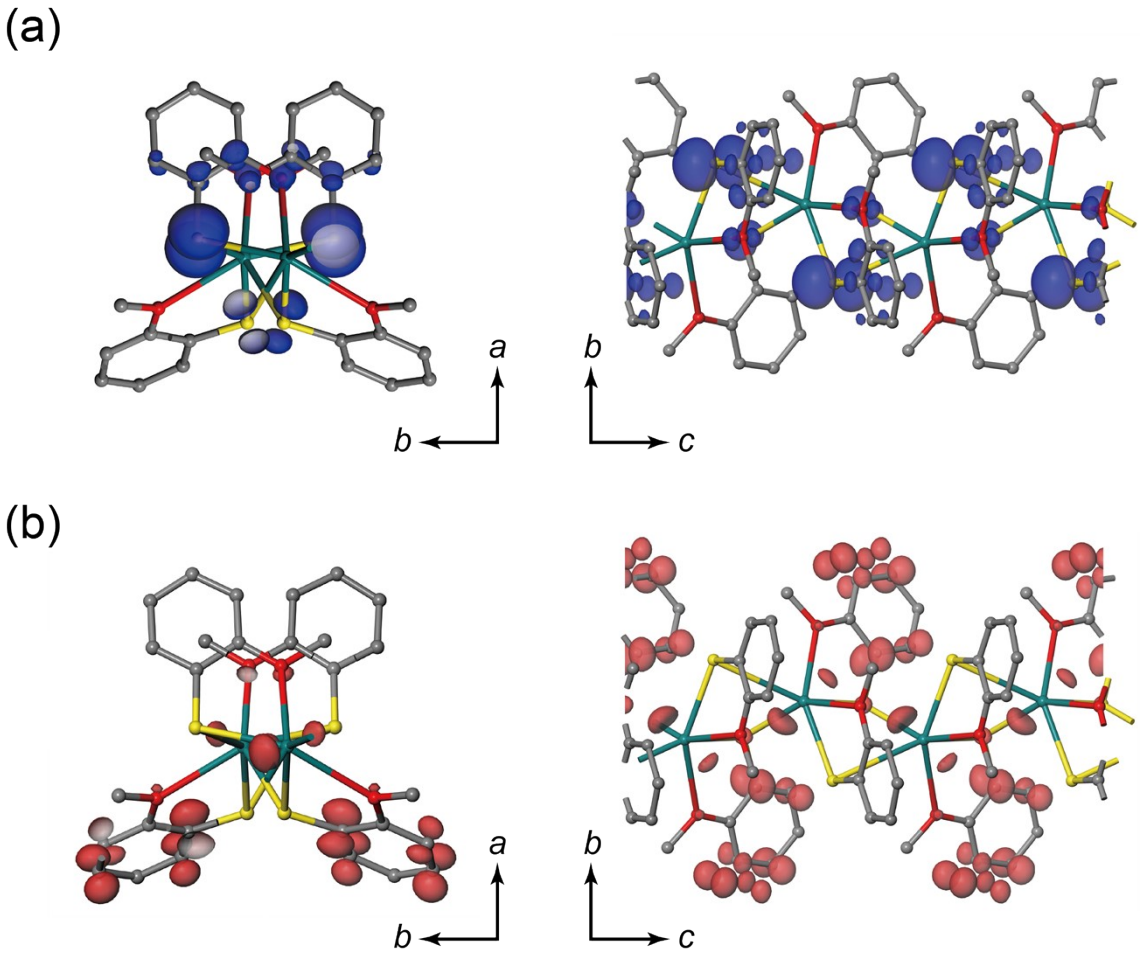

Fig. S15. Mapping of (a) VBM and (b) CBM for **KGF-32**.

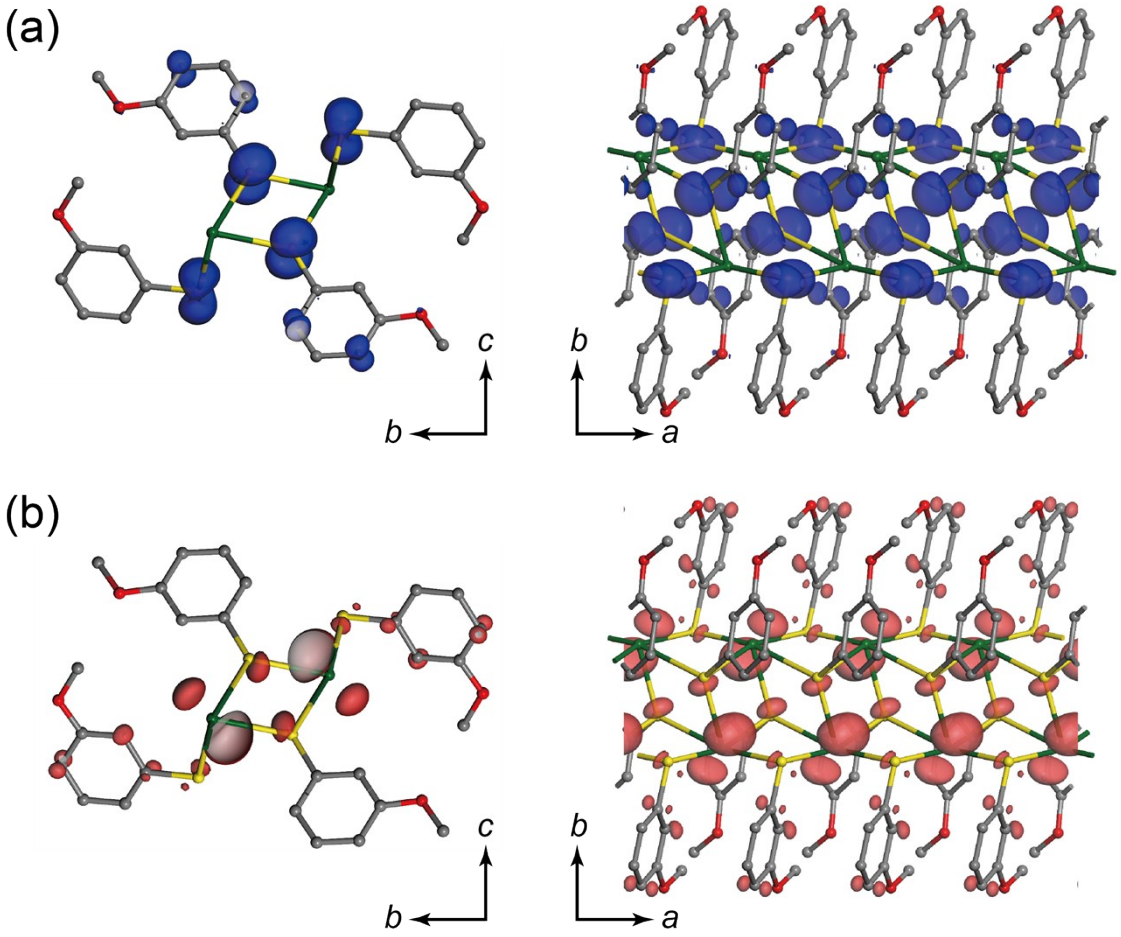

Fig. S16. Mapping of (a) VBM and (b) CBM for **KGF-33**.

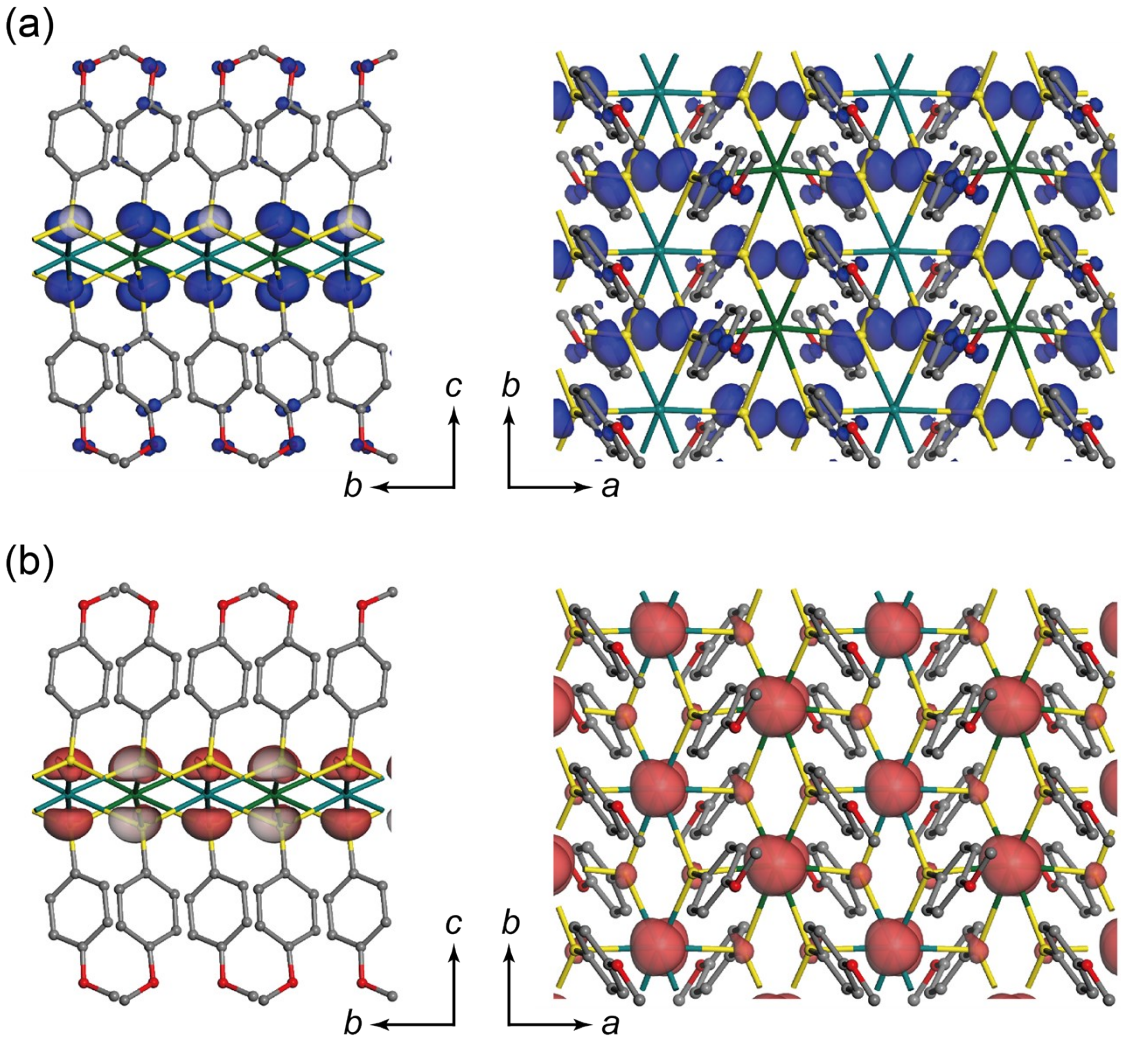

Fig. S17. Mapping of (a) VBM and (b) CBM for **KGF-34**.

Reference

S1. Y. Kamakura, P. Chinapang, S. Masaoka, A. Saeki, K. Ogasawara, S. R. Nishitani, H. Yoshikawa, T. Katayama, N. Tamai, K. Sugimoto, D. Tanaka, *J. Am. Chem. Soc.*, 2020, **142**, 27–32.

S2. Y. Kamakura, C. Sakura, A. Saeki, S. Masaoka, A. Fukui, D. Kiriya, K. Ogasawara, H. Yoshikawa, D. Tanaka, *Inorg. Chem.*, 2021, **60**, 5436–5441.

S3. Y. Kamakura, S. Fujisawa, K. Takahashi, H. Toshima, Y. Nakatani, H. Yoshikawa, A. Saeki, K. Ogasawara, D. Tanaka, *Inorg. Chem.*, 2021, **60**, 12691–12695.

S4. T. Wakiya, Y. Kamakura, H. Shibahara, K. Ogasawara, A. Saeki, R. Nishikubo, A. Inokuchi, H. Yoshikawa, D. Tanaka, *Angew. Chem. Int. Ed.*, 2021, **60**, 23217–23224.

S5. R. Akiyoshi, A. Saeki, K. Ogasawara, H. Yoshikawa, Y. Nakamura, D. Tanaka, *CrystEngComm*, 2023, **25**, 2990–2994.

S6. T. Okubo, H. Anma, N. Tanaka, K. Himoto, S. Seki, A. Saeki, M. Maekawa, T. Kuroda-Sowa, *Chem. Commun.*, 2013, **49**, 4316–4318.